Wearable Optical E-Tattoo for Deep Neck Hemodynamic Monitoring

Philip Tan
University of Texas at Austin
Austin, Texas, United States

Shreya Tamma
University of Texas at Austin
Austin, Texas, United States

Sarnab Bhattacharya
University of Texas at Austin
Austin, Texas, United States

James Tunnell
University of Texas at Austin
Austin, Texas, United States

Nanshu Lu*
University of Texas at Austin
Austin, Texas, United States
nanshulu@utexas.edu

ABSTRACT

Noninvasive detection of blood oxygen abnormalities in arteries and veins is crucial for determining sepsis, shock, and metabolic demand but is still unattainable. In this work, we devise a soft wearable e-tattoo sensor able to measure deep hemodynamics on the neck through photoplethysmography (PPG). There is widespread doubt that PPG cannot penetrate to the arteries and veins, a requirement to measure arterial and venous oxygenations (SaO_2 and SvO_2) directly. We investigate the penetration depth of PPG with computational and *in vitro* models. Finally, we demonstrate the e-tattoo's ability to distinguish arterial and venous pulses *in vivo*. These tests contradict the stereotype of PPG's poor penetration depth, substantiating the pursuit to optically measure arterial and venous pulses for SaO_2 and SvO_2 extraction.

CCS CONCEPTS

• **Hardware** → Emerging technologies → Biology-related information processing → Bio-embedded

KEYWORDS

Wearables; e-tattoos; PPG; biomedical instrumentation

ACM Reference format:

Philip Tan, Shreya Tamma, Sarnab Bhattacharya, James Tunnell, and Nanshu Lu. 2022. Optical Electronic Tattoo for Deep Hemodynamic Monitoring. In ACM/IEEE International Conference on Connected Health: Applications, Systems and Engineering Technologies (CHASE' 22), November 17–19, 2022, Washington, DC, USA. ACM, New York, NY, USA, 5 pages. https://doi.org/10.1145/3551455.3559604

ACM ISBN 978-1-4503-9476-5/22/11...$15.00
https://doi.org/10.1145/3551455.3559604

1 Introduction

Blood oxygenation is one of the most common biometrics measured in the clinical space. Typically, blood oxygenation is measured from the periphery (SpO_2) and thus only gives insight into local capillary blood oxygenation. Conversely, arterial and venous oxygenations (SaO_2 and SvO_2, respectively) remain an elusive biometric to measure noninvasively. SaO_2 and SvO_2 are necessary metrics to access the adequacy of the cardiopulmonary system. While widely used to assess tissue oxygenation, SpO_2 can only provide an assessment of local hypoxemia (low arterial blood oxygenation). Oxygen extraction is just as important for sustaining normal metabolic activity. Inadequate oxygen uptake by the tissue resulting in higher oxygenation in the venous blood is a symptom of severe sepsis and septic shock [1]. Continuous monitoring can help detect elevated levels of SvO_2, which has been correlated with increased mortality rates in septic shock patients [2]. However, the high cost and invasiveness of pulmonary artery and even central venous catheterization (PAC and CVC, respectively) [3] have led to decreased PAC usage and impassioned debates on if the benefits of such catheters outweigh the risks [3, 4].

Clearly, a non-invasive method of SvO_2 measurement is required. Previous attempts for non-invasive SvO_2 measurements have included analyzing the low-frequency signal components from a traditional photoplethysmography (PPG) sensor [5] and measuring mixed oxygen saturation of cerebral blood with near-infrared spectroscopy

[6]. However, these methods have critical flaws, including assuming that the low frequency signal is solely caused by venous blood movement and the inability to distinguish arterial and venous blood, respectively. Therefore, they have only demonstrated limited accuracy and have not seen practical adoption.

In this paper, we demonstrate a novel neck electronic tattoo (e-tattoo) that can monitor simultaneous arterial and venous pulse waveforms through PPG measurements. E-tattoos offer exciting opportunities for wearable medical devices by offering mechanical softness, thinness, and unsurpassable conformability. These attributes enable long-term monitoring, higher patient compliance, and unique measurement locations. Devices can couple to the skin purely with adhesion, getting rid of bulky straps. While straps or clips may be acceptable for the wrist, chest, or fingertip, sensitive locations such as the neck have so far been largely unexplored by wearables. With this tattoo, direct carotid artery and jugular vein measurement is possible.

Traditionally, however, it is claimed that PPG does not have a sufficient penetration depth to reach the arteries [7, 8]. Although other research has demonstrated that reflection PPG sensors on the neck can provide a pulse waveform signal [9], the exact mechanisms of signal origin is not clear. In support of the insufficient penetration depth theory, it is possible that the neck PPG signal is merely a motion artifact correlated with changes in arterial blood volume. Pulse oximetry measurements rely on differences in the absorption spectrums of chromophores (i.e., oxyhemoglobin and deoxyhemoglobin). Therefore, to spectroscopically analyze blood, light must directly pass through and interact with the blood. Accordingly, it is important to prove that light can reach the artery and diffuse back to the surface, as opposed to merely picking up secondary motion artifacts in the superficial tissues. In this work, we first provide computational and in vitro models proving that the penetration depth of our optical instrumentation is sufficient to interrogate arterial depths (i.e., > 1 cm).

Secondly, we demonstrate a change in waveform morphology based on PPG sensor position on the side of the neck. We hypothesize that the optical signal from the neck is a mixture of carotid artery and jugular vein signals. Although previous research has demonstrated changes in PPG waveform morphology based on sensing location [10, 11], a rigorous proof that the signal truly originates from deep hemodynamic activity is lacking.

2 Optical E-Tattoo

A custom e-tattoo wearable was used for in vivo and in vitro measurements (Figure 1). The e -tattoo contains two simultaneous, single wavelength (λ = 950 nm) source-detector pairs. Each detector's signal is amplified and filtered by a custom analog front end and digitized with an analog-to-digital converter Bluetooth microcontroller. The digitized signals are then transmitted over Bluetooth Low Energy to a custom Android mobile application.

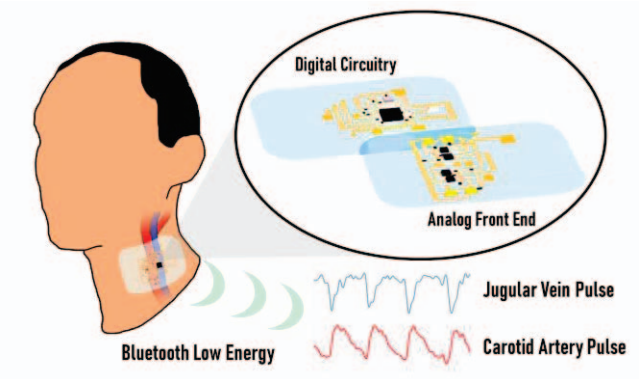

Figure 1 | Overview of neck wearable PPG e-tattoo. The e-tattoo consists of two diffuse reflectance sensors, an analog front end, and a Bluetooth Low Energy microprocessor. Simultaneous jugular vein and carotid artery pulse waveforms can be monitored.

3 Monte Carlo Light Propagation Models

In highly diffuse mediums, the relationship between emitted and measured light intensity (I_0 and I, respectively) is described by the Modified Beer-Lambert Law (MBLL)

$$\log\left(\frac{I}{I_0}\right) = \sum_i \varepsilon_i C_i D_a,$$

where ε and C refer to the extinction coefficient and concentration of a chromophore, respectively, and D_a is the differential pathlength.

If the penetration depth of light is sufficient, the concentration of hemoglobin in the optical sampling volume will increase during systole. This would result in a corresponding decrease in I. To estimate the optical sampling volume, the Photon Measurement Density Function (PMDF) was calculated using Monte Carlo simulations [12]. The PMDF is an estimation of the fluence from source to detector. The Monte Carlo method is used to numerically approximate the Radiative Transfer Equation (RTE) by launching individual photons and tracking their trajectories.

The tissue geometry consists of layers of epidermis, dermis, subcutaneous adipose, and muscle (Figure 2A). An artery composed of whole blood was set to a depth of 1 cm. The optical properties, absorption coefficient and reduced scattering coefficient, were calculated using equations by Jacques 2017 [13].

To calculate the PMDF, the fluence emitted from the source was obtained [14]. The tissue geometry was then shifted such that the source was located where the detector should be. A corresponding fluence distribution was collected with this new geometry. Finally, the PMDF was obtained by taking the geometric average of the two fluence distributions, voxel-wise (Figure 2B). The absorption in the optical path was then calculated as the estimated source-detector fluence multiplied by the absorption coefficient per voxel (Figure 2C). With this approach, we estimated the resultant absorption in the optical path by each voxel of tissue.

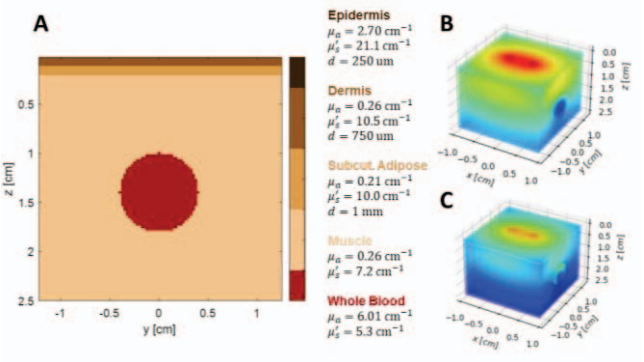

Figure 2 | Monte Carlo simulation setup. A, Cross-sectional tissue-vessel geometry and corresponding optical properties per tissue type. **B,** Example PMDF plot for SD = 6 mm. **C,** Example absorption in optical path plot for SD = 6 mm.

With source-detector distances between 4 and 12 mm, the contribution of absorption from the artery ranged between 15.6% and 21.5% (Figure 3A). Although not much light reaches the artery, the relatively high absorption of whole blood leads to significant influence from the artery on the total optical density.

To prove that changes in blood concentration in the sampling volume due vessel expansion and relaxation can be the origin of the PPG signal, a set of simulations with varying artery diameters was run. If light does not have sufficient penetration depth, no change in optical absorption would be observed when the vessel diameter is changed. In this simulation, there is no specular reflection or motion-related artifacts (e.g., compression of tissue).

For small changes in absorbance, the MBLL can be approximated as a linear relationship between changes in light intensity and absorption.

$$\log(1 + \Delta I) \approx \Delta I = \sum_i \varepsilon_i \Delta C_i D_a.$$

A strong linear correlation between vessel cross-sectional area and optical density (OD) was observed (r^2 = 0.995) (Figure 3B). This indicates that light does reach and is absorbed by the vessel, and the relationship between changes in arterial blood volume and observed light intensity can be explained by the MBLL.

4 Dynamic Optical Phantom Model

The penetration depth of PPG was tested using an in-vitro model. Optical phantoms were

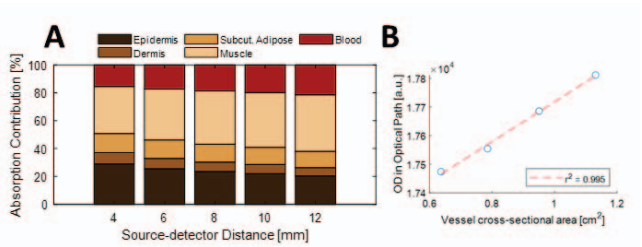

Figure 3 | Monte Carlo simulation results. A, Contribution of total absorption in the optical path for each tissue type. Multiple source-detector distances were tested. **B,** Artery radius vs. optical density in the optical path. As blood volume increases, absorbance also increases. This indicates that light does interact with the arterial blood.

fabricated with silicone rubber (Ecoflex, Smooth On) doped with Titanium Oxide (TiO_2) (PURE Supplement Co). The TiO_2 particles provided a reduced scattering coefficient (μ_s') of 1.2 mm^{-1} and were characterized using a diffuse reflectance spectrometer and a lookup table [15].

A hole was introduced through the phantoms at different depths to allow a non-distensible rubber tube to be inserted. Dyed water was used as fake blood. The tube acts as a blood vessel that does not induce motion in the system. Therefore, we can change the concentration of blood in the sampling volume without any correlated motion artifacts. A bi-directional pump was used to cyclically push-in and pull-out blood from the vessel (Figure 4). As air is replaced with the blood (and vice versa), the optical density of the phantom changes only at the depth of the artery.

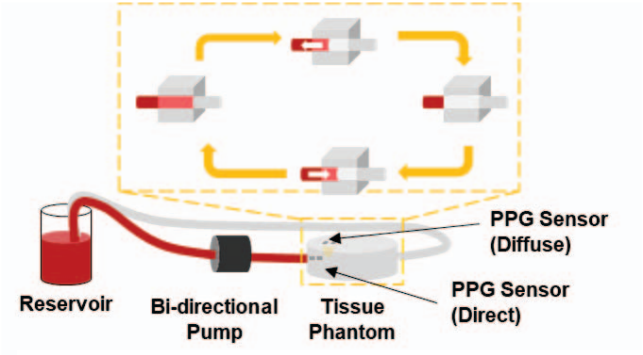

Figure 4 | Dynamic phantom setup. A bi-directional pump cycles dyed water in and out (f = 1 Hz) of a tissue phantom. A PPG sensor on the surface of the phantom records the diffuse reflected light intensity (labeled "Diffuse"). Another sensor was directly placed on the tube inside the phantom for inversion tests (labeled "Direct"). Blown-up yellow dashed box: a diagram of how the dyed water enters and leaves the phantom.

To prove that the signal we obtained was solely from changes in optical absorbance, we used signal-to-noise ratio (SnR) to gauge how much of the signal came from extraneous factors. The reference noise signal was generated by using the bi-directional pump as before but without air in the vessel. The fluid still oscillated back and forth within the phantom, but the total concentration of the fluid did not change inside the phantom. As a result, the reference noise signal contained the same motor vibration, EMI, and ambient light signal but no signal from changes in optical absorbance. The high observed SnR (> 80 dB for all depths) indicate that the signal is not caused by motion or extraneous factors (Figure 5).

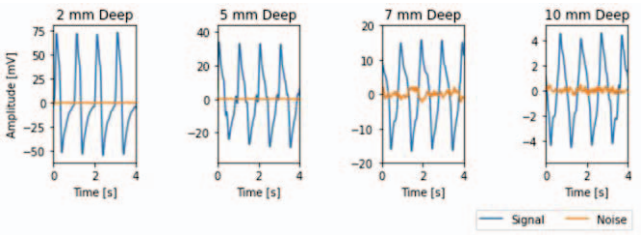

Figure 5 | Signal-to-noise ratio. To test if the optical signal could have been influenced by factors other than the absorbance in the phantom, the signal-to-noise ratio was calculated to be over 80 dB. The noise reference was measured with the same phantom, motor, vessel, and sensor set up, but without the air gap in the vessel.

The position-dependent PPG waveform was previously suggested to be caused by changes in the light-tissue interaction [16]. Specifically, they hypothesized that changes in position could alter whether absorbance or specular reflection dominates. If specular reflection dominates, greater blood volume could lead to increased measured light intensity and results in an "inverted" waveform. If this hypothesis is true, then waveform changes from placing the PPG sensor on different locations on the neck may not be caused by the jugular or carotid vessels. Here, we placed one sensor directly on the vessel and another on the surface phantom. The second sensor measures the diffuse reflection signal from different lateral positions (0 to 20 mm in 5 mm increments). No inversion was observed in any lateral position (Figure 6). This suggests that lateral position is not the cause of waveform shape modulation.

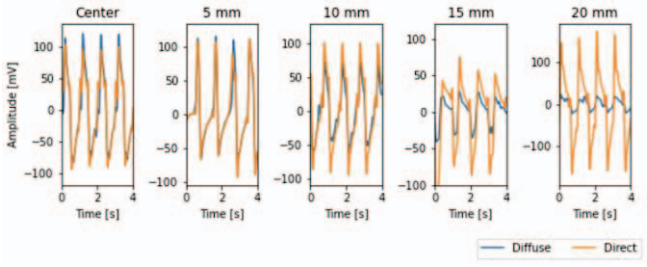

Figure 6 | Diffuse reflectance signal vs. lateral position. We tested if signal inversion could be caused solely by lateral position of the sensor relative to the vessel. One PPG sensor was placed directly on the vessel inside the phantom (Direct) and another was placed on the surface of the phantom (Diffuse). None of the lateral positions led to inverted waveforms.

5 In Vivo Measurement of Carotid and Jugular Pulses

To demonstrate the superimposed arterial and venous optical signals, 12 evenly spaced (pitch = 5 mm) locations were marked on a subject's neck (Figure 7). For each location, the tattoo recorded 30 seconds of simultaneous PPG and electrocardiogram (ECG) data while the subject was at rest. The R-peak from the ECG signal indicates the start of ventricular contraction and was used to segment the PPG waveforms. Each cardiac cycle was normalized in time, bandpass filtered (1-10 Hz), and used to calculate a grand average waveform at each location (Figure 8).

Figure 7 | *In vivo* placements of the e-tattoo on the neck. PPG signals were obtained from different locations on the neck to observe the changes in waveform morphology.

As the sensor is moved posteriorly, we observe the following waveform morphology changes: First, a large descent begins to appear ~20% in the cardiac cycle. We hypothesize that this corresponds with atrial filling, thus representing the venous x descent. Both the descent and peaks occur later in the posterior locations.

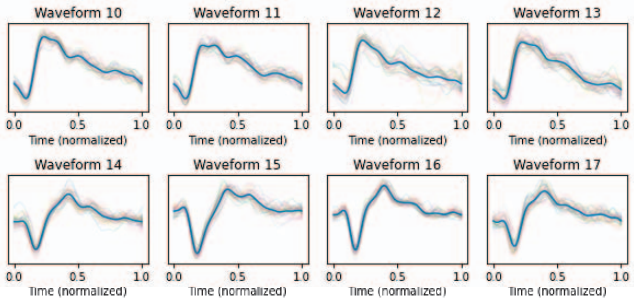

Figure 8 | PPG signal vs. position on neck. One minute of PPG signals was recorded at each location. Waveforms were segmented by the R peaks from a synchronous ECG recording and normalized by period. The dark curve is the grand average of all waveforms.

6 Conclusion

This paper presents a noninvasive and wireless neck-mounted e-tattoo to measure arterial and venous pulse waveforms continuously and simultaneously using PPG. We constructed computational and *in vitro* models to prove that changes in arterial blood volume are sufficiently detectable with PPG. By placing the e-tattoo at different positions across the neck, we have also detected changes in waveform morphology, contributing to existing literature on the interaction of light with the jugular and carotid vessels. This project serves as a proof-of-concept for using PPG to interrogate arterial and venous blood.

ACKNOWLEDGMENTS

This research is sponsored by the US Army Research Office under Grant No. W911NF-18-2-0270.

REFERENCES

1. Textoris, J., et al., High central venous oxygen saturation in the latter stages of septic shock is associated with increased mortality. Critical Care, 2011. **15**(4): p. R176.
2. Pope, J.V., et al., Multicenter Study of Central Venous Oxygen Saturation (ScvO2) as a Predictor of Mortality in Patients With Sepsis. Annals of Emergency Medicine, 2010. **55**(1): p. 40-46.e1.
3. Vincent, J.-L., et al., The pulmonary artery catheter: In medio virtus. Critical Care Medicine, 2008. **36**(11).
4. Wiener, R.S. and H.G. Welch, Trends in the Use of the Pulmonary Artery Catheter in the United States, 1993-2004. JAMA, 2007. **298**(4): p. 423-429.
5. Walton, Z.D., et al., Measuring venous oxygenation using the photoplethysmograph waveform. Journal of Clinical Monitoring and Computing, 2010. **24**(4): p. 295-303.
6. Schmidt, C., et al., The effects of systemic oxygenation on cerebral oxygen saturation and its relationship to mixed venous oxygen saturation: A prospective observational study comparison of the INVOS and ForeSight Elite cerebral oximeters. Canadian Journal of Anesthesia/Journal canadien d'anesthésie, 2018. **65**(7): p. 766-775.
7. Lee, G.-H., et al., Multifunctional materials for implantable and wearable photonic healthcare devices. Nature Reviews Materials, 2020. **5**(2): p. 149-165.
8. Ibrahim, B., D.A. Hall, and R. Jafari, Pulse Wave Modeling Using Bio-Impedance Simulation Platform Based on a 3D Time-Varying Circuit Model. IEEE Transactions on Biomedical Circuits and Systems, 2021. **15**(1): p. 143-158.
9. Nabeel, P.M., et al. Experimental validation of dual PPG local pulse wave velocity probe. in 2017 IEEE International Symposium on Medical Measurements and Applications (MeMeA). 2017.
10. Amelard, R., et al., Non-contact hemodynamic imaging reveals the jugular venous pulse waveform. Scientific reports, 2017. **7**: p. 40150-40150.
11. García-López, I. and E. Rodriguez-Villegas, Extracting the Jugular Venous Pulse from Anterior Neck Contact Photoplethysmography. Scientific Reports, 2020. **10**(1): p. 3466.
12. Jacques, S., T. Li, and S. Prahl, mcxyz. 2019.
13. Jacques, S.L., Optical properties of biological tissues: a review. Physics in Medicine and Biology, 2013. **58**(11): p. R37-R61.
14. Sabrina, B. and J.C. Robert, How short is short? Optimum source–detector distance for short-separation channels in functional near-infrared spectroscopy. Neurophotonics, 2015. **2**(2): p. 1-9.
15. Ricky, J.H., et al., Monte Carlo lookup table-based inverse model for extracting optical properties from tissue-simulating phantoms using diffuse reflectance spectroscopy. Journal of Biomedical Optics, 2013. **18**(3): p. 1-5.
16. Weinman, J., A. Hayat, and G. Raviv, Reflection photoplethysmography of arterial-blood-volume pulses. Medical and Biological Engineering and Computing, 1977. **15**(1): p. 22-31.